Progress In Electromagnetics Research, Vol. 153, 69–91, 2015

Numerical Study of a Time-Domain Finite Element Method for Nonlinear Magnetic Problems in Three Dimensions

Su Yan[1, 2, *], Jian-Ming Jin[1], Chao-Fu Wang[3], and Joseph Kotulski[4]

(*Invited Paper*)

Abstract—In this work, numerical analysis of nonlinear ferromagnetic problems is presented using the three-dimensional time-domain finite element method (TDFEM). Formulated with the second-order nonlinear partial differential equation (PDE) combined with the inverse Jiles-Atherton (J-A) vector hysteresis model, the nonlinear problems are solved in the time domain with the Newton-Raphson method. To solve the ordinary differential equation (ODE) representing the magnetic hysteresis accurately and efficiently, several ODE solvers are specifically designed and investigated. To improve the computational efficiency of the Newton-Raphson method, the multi-dimensional secant methods, aka Broyden's methods, are incorporated in the nonlinear TDFEM solver. A nonuniform time-stepping scheme is also developed using the weighted residual approach to remove the requirement of a uniform time-step size during the simulation. The capability and the performance of the proposed methods are demonstrated by various numerical examples.

1. INTRODUCTION

Magnetic hysteresis and constitutive nonlinearity are fundamental properties of ferromagnetic materials. Mathematically speaking, the magnetization intensity is not only a nonlinear, but also a multi-valued function of the magnetic field. The magnetic susceptibility depends on both the current and the past values of the magnetic field. Because of their constitutive nonlinearity, ferromagnetic materials have found a wide range of applications in data storage and processing, electric power generation, telecommunications, and transducers in smart systems. The optimal design of a ferromagnetic device requires an accurate solution of the nonlinear magnetic problem with proper material and electromagnetic models.

In our previous work [1], a numerical solution to the nonlinear magnetic problem is formulated with a three-dimensional time-domain finite element method (TDFEM) [2] combining with the inverse vector Jiles-Atherton (J-A) model [3–6]. The physical problem is expressed as a nonlinear second-order partial differential equation (PDE) in the time domain, which is solved using the Newton-Raphson or Newton-like methods. To properly model the nonlinear ferromagnetic materials, the well-known J-A model is employed. In the J-A model, the constitutive relation of the ferromagnetic materials is described in terms of an ordinary differential equation (ODE), which can be solved with a proper time integration method. The solution of the coupled PDE-ODE system is a nonlinear iterative process. In order to solve the nonlinear PDE using the Newton-Raphson method, an estimated solution of the magnetic

Received 10 September 2015, Accepted 18 October 2015, Scheduled 21 October 2015

* Corresponding author: Su Yan (suyan@illinois.edu).

[1] Center for Computational Electromagnetics, Department of Electrical and Computer Engineering, University of Illinois at Urbana-Champaign, Urbana, IL 61801-2991, USA. [2] Department of Microwave Engineering, University of Electronic Science and Technology of China, Chengdu, Sichuan 610054, China. [3] National University of Singapore, Singapore 117411, Singapore. [4] Sandia National Laboratories, Albuquerque, NM 87123, USA.

flux is provided and fed into the ODE, from which the differential reluctivity and the magnetic field are calculated and returned back to the PDE to generate the next estimated solution. This process continues iteratively until convergence is achieved.

Since the ODE describing the magnetic hysteresis represents a mathematically stiff problem, it is inefficient to solve numerically because the rapidly varying component of the solution forces the use of very small step sizes to maintain stability. Unfortunately, the step size is not controllable in the nonlinear time-domain formulation because it is determined by the nonlinear PDE solver. In this paper, the accurate and efficient solution of the stiff ODE is discussed, and different methods are discussed and compared.

Once the constitutive relation is obtained accurately and efficiently, the PDE that describes the nonlinear magnetic problem can be solved with the TDFEM using the Newton-Raphson method. An obvious advantage of the Newton-Raphson method is its local quadratic convergence when starting from an initial estimation that is sufficiently close to the true solution. A quadratic convergence means that the error of the solution reduces quadratically with iterations, or a two-digit precision gain per Newton iteration. Theoretically, to achieve a relative residual of 10^{-8} in a quadratically converging process, only four Newton iterations are needed, which makes the Newton-Raphson method very attractive. Solving the nonlinear magnetic problems in the time domain with the Newton-Raphson method has two obvious advantages. The first advantage is that the time-domain solver has a natural choice of the initial guess, which is the solution at the preceding time step. As a result, the convergence of the time-domain solver can always be achieved if the time-step size is small enough such that the solutions at two successive time steps are sufficiently close. The second advantage of the time-domain solver is the ability to capture all the physical phenomena in a real process, such as higher-order harmonic responses, magnetic remanence, and hysteresis losses. In the meantime, there are also several challenges in the time-domain modeling of nonlinear magnetic problems. One such challenge comes from the application of the Newton-Raphson method, where the Jacobian matrix needs to be updated and solved at every nonlinear iteration, which makes the solution very time consuming for large problems.

In order to improve the efficiency of the Newton-Raphson method, the Jacobian matrix and its inverse can be formed approximately and implicitly at each Newton step using the multi-dimensional secant updating methods, also known as Broyden's methods [7]. Broyden's methods can reduce the computational cost by using function values at successive iterations to build an approximation of the Jacobian matrix and avoiding any explicit evaluation of the derivatives. The computational cost can be further reduced with Broyden's methods by updating the factorization of the approximated Jacobian matrix rather than refactoring it repeatedly at each Newton step. In this paper, Broyden's methods are introduced and employed to reduce the computational cost while maintaining a fast convergence, which is usually super-linear because of the approximation.

To achieve a fast convergence, the time-step size of the nonlinear time-domain solver needs to be small enough. In the TDFEM, the time-step size is usually a constant throughout the entire simulation. However, there are many situations where the application of nonuniform time-step sizes is more desirable. For example, when the excitation signal is varying rapidly, a small time-step size should be used in order to capture fast variations in physical quantities and guarantee convergence. But when the excitation signal is varying slowly, it is much more efficient if a larger time-step size is adopted. As a result, the use of nonuniform time-step sizes would be a better choice in real applications. Another scenario where a nonuniform time-stepping is more appropriate is the simulation of the magnetic hysteresis phenomenon. Since the nonlinear hysteresis is a stiff mathematical problem, when the amplitude of the externally applied excitation is high, the magnetic field would change very drastically. But when the amplitude of the excitation is low, the magnetic field would change quite smoothly. As a result, it is not always necessary to use a uniformly small time-step size throughout the entire time-marching process. In this paper, a nonuniform time-stepping scheme is developed using the weighted residual approach [8] to remove the requirement of a uniform time-step size during the simulation.

This paper is organized as follows. In Section 2, the TDFEM formulation for the nonlinear magnetic problems is briefly reviewed and validated through several benchmark problems. Different approaches of solving the ODE representing the constitutive hysteresis are discussed and their accuracy and efficiency are compared in Section 3. To alleviate the computational bottleneck of constructing and solving the Jacobian matrix equation, Broyden's methods are incorporated in the nonlinear TDFEM

solver in Section 4. In Section 5, the nonuniform time-stepping scheme is developed and its numerical performance is investigated. The applications of the proposed nonlinear solver are demonstrated through the investigation of magnetic hysteresis and its nonlinear effects in Section 6. Conclusion is drawn in Section 7.

2. TDFEM FORMULATIONS FOR NONLINEAR MAGNETIC PROBLEMS

In this section, we briefly review the nonlinear inverse J-A hysteresis model [6] and the TDFEM formulation for nonlinear magnetic problems developed in [1], and present simple numerical examples for validation.

2.1. Inverse Vector Jiles-Atherton Model

In the inverse vector J-A model [6], the magnetic field $\mathbf{H}$ and the magnetization $\mathbf{M}$ are formulated as functions of the magnetic flux $\mathbf{B}$

$$d\mathbf{M} = \nu_0 \bar{\boldsymbol{\xi}}_r^d(\mathbf{B},\mathbf{H}) \cdot d\mathbf{B} \tag{1}$$

$$d\mathbf{H} = \nu_0 \bar{\boldsymbol{\nu}}_r^d(\mathbf{B},\mathbf{H}) \cdot d\mathbf{B}, \tag{2}$$

where $\nu_0 = 1/\mu_0$ is the reluctivity in free-space, $\bar{\boldsymbol{\xi}}_r^d$ is the relative differential magnetizability tensor, and $\bar{\boldsymbol{\nu}}_r^d$ is the relative differential reluctivity tensor. The detailed expression for $\bar{\boldsymbol{\xi}}_r^d$ can be found in [1]. Since

$$\mathbf{B} = \mu_0(\mathbf{H} + \mathbf{M}), \tag{3}$$

the differential reluctivity and magnetizability tensors can be related as

$$\bar{\boldsymbol{\nu}}_r^d = \bar{\mathbf{I}} - \bar{\boldsymbol{\xi}}_r^d, \tag{4}$$

where $\bar{\mathbf{I}}$ is the unit tensor. From these differential relations, the magnetization $\mathbf{M}$ and the magnetic field $\mathbf{H}$ can be determined by the value and variation of the magnetic flux $\mathbf{B}$.

2.2. Nonlinear Time-Domain Finite Element Formulation

The proposed TDFEM formulation for nonlinear magnetic problems solves for the magnetic vector potential $\mathbf{A}$, which satisfies the second-order curl-curl equation as

$$\nabla \times (\nu_r \nabla \times \mathbf{A}) + \frac{\varepsilon_r}{c_0^2}\frac{\partial^2}{\partial t^2}\mathbf{A} + \frac{\eta_0}{c_0}\sigma\frac{\partial}{\partial t}\mathbf{A} = \mu_0 \mathbf{J}_{\text{imp}}, \tag{5}$$

where ε_r and ν_r are the relative permittivity and reluctivity of the material, η_0 and c_0 are the intrinsic impedance and the speed of light in free-space, respectively. Since it is usually solenoidal in magnetic problems, the impressed current $\mathbf{J}_{\text{imp}}$ can be expressed in terms of the impressed current vector potential $\mathbf{T}_{\text{imp}}$ [9] as $\mathbf{J}_{\text{imp}} = \nabla \times \mathbf{T}_{\text{imp}}$, which is equivalent to enforcing a gauge condition on $\mathbf{A}$.

The unknown vector $\mathbf{A}$ can be spatially expanded in terms of vector basis functions $\mathbf{N}_j$ [10–12], and temporally discretized using the Newmark-β method [8, 13, 14] with $\beta = 1/4$. The curl-curl Equation (5) can therefore be discretized as

$$\begin{aligned}
&\left\{\frac{1}{4}c_0^2\Delta t^2[S] + [M] + \frac{1}{2}\eta_0 c_0 \Delta t[G] + \frac{1}{2}c_0\Delta t[A]\right\}\{a\}^{n+1} \\
&= -\left\{\frac{1}{2}c_0^2\Delta t^2[S] - 2[M]\right\}\{a\}^n - \left\{\frac{1}{4}c_0^2\Delta t^2[S] + [M] - \frac{1}{2}\eta_0 c_0\Delta t[G] - \frac{1}{2}c_0\Delta t[A]\right\}\{a\}^{n-1} \\
&\quad + \eta_0 c_0 \Delta t^2\left(\frac{1}{4}\{b\}^{n+1} + \frac{1}{2}\{b\}^n + \frac{1}{4}\{b\}^{n-1}\right),
\end{aligned} \tag{6}$$

where

$$S_{ij} = \iiint_V \nu_r \left(\nabla \times \mathbf{N}_i\right) \cdot \left(\nabla \times \mathbf{N}_j\right) dV \tag{7}$$

$$M_{ij} = \iiint_V \varepsilon_r \mathbf{N}_i \cdot \mathbf{N}_j dV \tag{8}$$

$$G_{ij} = \iiint_V \sigma \mathbf{N}_i \cdot \mathbf{N}_j dV \tag{9}$$

$$A_{ij} = \iint_S \frac{1}{\eta_r} (\hat{\mathbf{n}} \times \mathbf{N}_i) \cdot (\hat{\mathbf{n}} \times \mathbf{N}_j) \, dS \tag{10}$$

$$b_i = \iiint_V (\nabla \times \mathbf{N}_i) \cdot \mathbf{T}_{\text{imp}} dV. \tag{11}$$

In the above expressions, $\mathbf{N}_i$ and $\mathbf{N}_j$ represent vector basis functions, V is the solution domain, $S = \partial V$ is the boundary of V, and η_r is the relative impedance on the truncation boundary [15, 16]. Equation (6) can be solved step by step by marching from the known solutions at the $(n-1)$th and the nth time steps to the $(n+1)$th time step. Once the magnetic vector potential $\mathbf{A}$ is obtained at some time step t_{n+1}, the magnetic flux $\mathbf{B}$ and electric field $\mathbf{E}$ at the same time step can be calculated.

Since the relative reluctivity of the material ν_r is a function of the magnetic flux density, which is a function of the unknown vector $\{a\}^{n+1}$, the system Equation (6) is nonlinear. Such a nonlinear system can be solved iteratively by using the polarization technique and the Newton-Raphson method as [1]

$$[J]\{\delta a\} = -\{r\} \tag{12}$$

$$\{a\}_{k+1}^{n+1} = \{a\}_k^{n+1} + \{\delta a\}. \tag{13}$$

In (12), $\{r\}$ is the residual function at the kth Newton step

$$\{r\} = [K_p]^{n+1}\{a\}_k^{n+1} + [K_p]^n\{a\}^n + [K_p]^{n-1}\{a\}^{n-1} + \{R\}_k - \{\tilde{b}\}, \tag{14}$$

where

$$[K_p]^{n\pm1} = \frac{1}{4}c_0^2\Delta t^2[S_p] + [M] \pm \frac{1}{2}\eta_0 c_0 \Delta t[G] \pm \frac{1}{2}c_0\Delta t[A] \tag{15}$$

$$[K_p]^n = \frac{1}{2}c_0^2\Delta t^2[S_p] - 2[M] \tag{16}$$

$$\{\tilde{b}\} = \eta_0 c_0 \Delta t^2 \left(\frac{1}{4}\{b\}^{n+1} + \frac{1}{2}\{b\}^n + \frac{1}{4}\{b\}^{n-1}\right) \tag{17}$$

and the nonlinearity is presented in

$$R_{k,i} = \mu_0 c_0^2 \Delta t^2 \iiint_V (\nabla \times \mathbf{N}_i) \cdot \mathbf{R}_k dV, \tag{18}$$

where $\mathbf{R}_k$ is a nonlinear function of the vector potential $\mathbf{A}$ at the kth Newton step

$$\mathbf{R}(\mathbf{A}) = \mathbf{H} - \nu_r^{\text{opt}}\nu_0\mathbf{B}, \tag{19}$$

in which $\mathbf{H}$ is obtained from the J-A model presented in Section 2.1, and ν_r^{opt} is a constant, which can be chosen as [1]

$$\nu_r^{\text{opt}} = \begin{cases} \nu_r, & \text{in the linear material} \\ 0, & \text{in the nonlinear material.} \end{cases}$$

With the definition of ν_r^{opt}, the stiffness matrix $[S_p]$ can be calculated as

$$S_{p,ij} = \iiint_V \nu_r^{\text{opt}} (\nabla \times \mathbf{N}_i) \cdot (\nabla \times \mathbf{N}_j) \, dV. \tag{20}$$

In (12), $[J]$ is the Jacobian matrix at the kth Newton step

$$[J] = \frac{1}{4}c_0^2\Delta t^2[S^J] + [M] + \frac{1}{2}\eta_0 c_0 \Delta t[G] + \frac{1}{2}c_0\Delta t[A]. \tag{21}$$

If the constitutive relation of the ferromagnetic material is described by a scalar relation $\mathbf{H} = \nu_0\nu_r(B)\mathbf{B}$, where $B = \|\mathbf{B}\|$,

$$S_{ij}^J = \iiint_V \left\{\nu_r (\nabla \times \mathbf{N}_i) \cdot (\nabla \times \mathbf{N}_j) + \left(\nu_r^d - \nu_r\right)\left[(\nabla \times \mathbf{N}_i) \cdot \frac{\mathbf{B}}{B}\right]\left[(\nabla \times \mathbf{N}_j) \cdot \frac{\mathbf{B}}{B}\right]\right\} dV. \tag{22}$$

If the constitutive relation of the ferromagnetic material is described by a vector relation $\mathbf{H} = \nu_0 \bar{\boldsymbol{\nu}}_r(\mathbf{B}) \cdot \mathbf{B}$,

$$S_{ij}^{J} = \iiint_V (\nabla \times \mathbf{N}_i) \cdot \bar{\boldsymbol{\nu}}_r^d \cdot (\nabla \times \mathbf{N}_j)\, dV. \tag{23}$$

Besides the Newton-Raphson method, the nonlinear system matrix (6) can also be solved with a simple fixed-point method where $\mathbf{A}$ can be solved with a fixed-point iteration

$$\nabla \times \left(\nu_r^{\text{opt}} \nabla \times \mathbf{A}\right) + \frac{\varepsilon_r}{c_0^2} \frac{\partial^2}{\partial t^2} \mathbf{A} + \frac{\eta_0}{c_0} \sigma \frac{\partial}{\partial t} \mathbf{A} = \mu_0 \mathbf{J}_{\text{imp}} - \mu_0 \nabla \times \mathbf{R}. \tag{24}$$

The solution process has been described in [1] and will not be repeated in this paper.

2.3. Benchmark and Validation

To demonstrate the validity of the proposed formulations and compare the performance of the Newton-Raphson and fixed-point methods, we consider two benchmark problems, which are adopted from the "testing electromagnetic analysis methods" (TEAM) workshop [17]. Since the excitation current has a majority of energy concentrating at very low frequencies or even at dc, the tree-cotree splitting (TCS) [18, 19] has been applied to the TDFEM solver, in order to eliminate the low-frequency breakdown problem. To deal with the multiscale geometric configuration, higher-order hierarchical vector basis functions [12, 20] are also employed whenever needed to achieve a better accuracy.

2.3.1. TEAM Problem 10

The first problem considered is the TEAM workshop problem 10 as shown in Fig. 1, where a racetrack coil is placed between two steel channels and a flat steel plate is inserted in between of these two channels. The steel channels and plate have a relative permittivity of $\varepsilon_r = 1.0$, a conductivity of $\sigma = 7.505 \times 10^6\,\text{S/m}$, and a permeability given by the nonlinear B-H relation through discrete measurement data, from which the scalar constitutive relation is constructed and shown in Fig. 2(a) in [1]. Since it is a scalar B-H relation, the nonlinear TDFEM formulation (22) is used for this example. The steel structure is excited with a dc coil current turned on from 0 A and gradually increased to I_m. The magnetic flux in three different regions S_1, S_2, and S_3 are recorded and compared with measurement data. This problem is simulated using both the Newton-Raphson and the fixed-point methods and a good agreement is achieved between the measurement and the simulated results [1]. Here, we compare the computational performance between the two methods. As shown in Tab. 1, it can be seen that

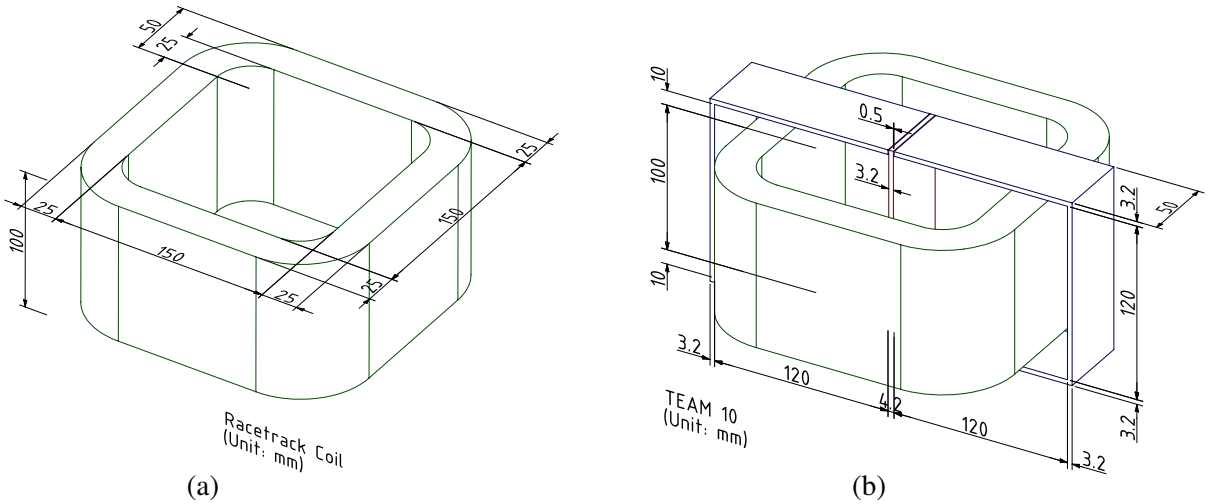

Figure 1. Problem setting and dimensions of TEAM problem 10. (a) Racetrack coil. (b) Steel channels and center plate.

Table 1. Comparison of computational data for solving TEAM problem 10 using Newton-Raphson (NR) and fixed-point (FP) methods.

$I_m = 18.52\,\mathrm{A}$	Δt (ms)	Total Time Steps	Ave. Iter. Per Time Step	Total CPU Time (s)
NR	1.0	200	3.03	1698.18
FP	1.0	200	12.91	1051.52

Table 2. Comparison of computational data for solving TEAM problem 10 using Newton-Raphson (NR) method with different time-step sizes.

$I_m = 5.64\,\mathrm{A}$	Δt (ms)	Total Time Steps	Ave. Iter. Per Time Step	Total CPU Time (s)
NR	0.15	1000	2.01	7518.15
NR	3.0	50	3.04	425.77

for this specific problem, the fixed-point method requires less computational time than the Newton-Raphson method, because it does not require the construction and solution of the Jacobian matrix. However, the average number of iterations needed for the fixed-point method to converge at each time step is significantly larger than that for the Newton-Raphson method, which means that the fixed-point method is much more difficult to converge. In a more complicated application, the fixed-point method would require a much smaller time-step size in order to achieve convergence. Ideally, a larger time-step size is more desirable in real applications because it is much more efficient in reducing the total computational time. This can be seen very clearly from Tab. 2, where the computational costs needed by the Newton-Raphson method with different Δt are compared. Although a smaller Δt can converge with a smaller number of Newton iterations per time step, the larger number of time steps eventually counteracts the computational time reduction and results in a larger time consumption.

2.3.2. TEAM Problem 13

Next, we consider TEAM benchmark problem 13 [21]. Compared with TEAM problem 10, problem 13 has the same excitation coil as that shown in Fig. 1(a). The difference is that the steel channels in problem 13 are shifted horizontally to both sides, as shown in Fig. 2(a). The steel structure is then excited with a 1000-AT coil current. The unit AT is usually used in the magnetics community to express

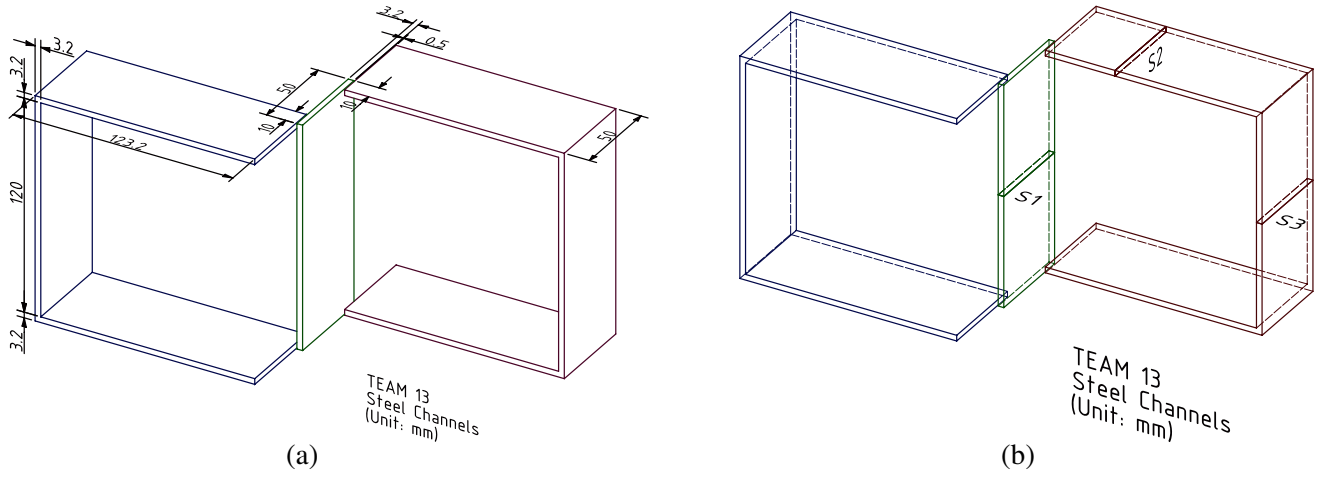

Figure 2. Problem setting and dimensions of the steel channels and center plate in TEAM problem 13. (a) Steel channels and center plate. (b) Observation areas on the steel channels.

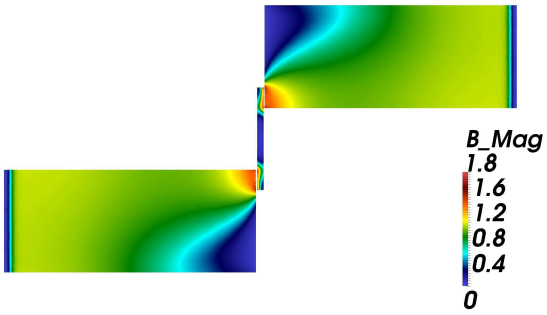

Figure 3. Magnitude of the magnetic flux density on the surface of the steel structure in TEAM problem 13, top view.

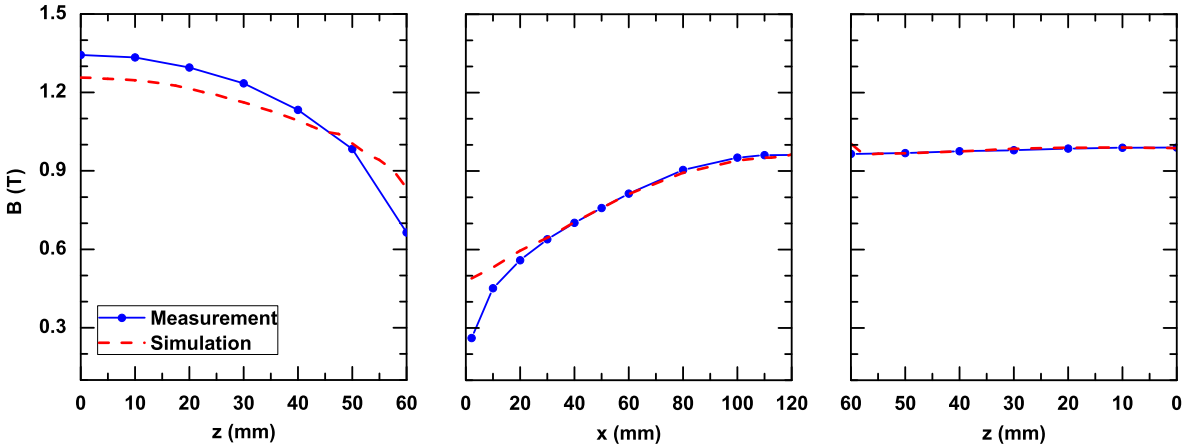

Figure 4. Numerical results of TEAM problem 13 with 1000-AT coil current excitation. Average magnetic flux density in the observation areas S_1, S_2, and S_3 is shown as a function of position.

the magnitude of the total coil current, which stands for Ampere turn, and is defined as the product of I_m and the number of turns of the coil. The top view of the magnitude of the magnetic flux density is shown in Fig. 3 when it reaches to the steady state. The average magnitude of the magnetic flux density in three different areas shown in Fig. 2(b) are recorded as functions of position. The comparison between the results obtained by the proposed nonlinear TDFEM solver and the measurement data [17] is shown in Fig. 4. A good agreement can be observed from these figures.

3. ORDINARY DIFFERENTIAL EQUATION SOLVERS FOR MAGNETIC HYSTERESIS

From the nonlinear TDFEM formulations presented in the preceding section, it is clear that to model the magnetic hysteresis phenomenon, the accurate generation of $\bar{\boldsymbol{\nu}}_r^d$ and $\mathbf{H}$ is critical to the fast convergence of the Newton-Raphson method. Since in the hysteresis model introduced in Section 2.1, the constitutive relation is described in terms of ODEs as those shown in (1) and (2), the question now becomes how these ODEs can be solved accurately and efficiently. In this section, the accurate solution of the ODE (2) is discussed because the relative differential reluctivity $\bar{\boldsymbol{\nu}}_r^d$ is used in the TDFEM formulation (23). Specifically, Euler's method and the Runge-Kutta method are investigated. Other more sophisticated methods that are used to solve ODEs can also be applied to (2) in a similar manner.

3.1. Euler's Method

The simplest method that is commonly used to solve an ODE is Euler's method, in which the first-order Taylor series expansion is applied to achieve

$$\mathbf{H}\left(\mathbf{B}+\Delta\mathbf{B}\right) \approx \mathbf{H}(\mathbf{B}) + \frac{\partial \mathbf{H}}{\partial \mathbf{B}} \cdot \Delta\mathbf{B} = \mathbf{H}(\mathbf{B}) + \nu_0 \bar{\boldsymbol{\nu}}_r^d(\mathbf{B},\mathbf{H}) \cdot \Delta\mathbf{B}. \tag{25}$$

The magnetic field $\mathbf{H}$ can therefore be obtained as

$$\mathbf{H}_k^{n+1} = \mathbf{H}^n + \nu_0 \bar{\boldsymbol{\nu}}_r^d\left(\mathbf{B}^n,\mathbf{H}^n\right) \cdot \left(\mathbf{B}_k^{n+1} - \mathbf{B}^n\right), \tag{26}$$

where $\mathbf{H}^n$ and $\mathbf{B}^n$ are the solutions from the previous time step n, and $\mathbf{B}_k^{n+1}$ is the estimated solution at the kth Newton iteration of the current time step $n+1$, which is produced from the TDFEM solver. From the above equation, the estimated magnetic field $\mathbf{H}_k^{n+1}$ can be obtained and fed back into the TDFEM solver for the solution of the next estimation $\mathbf{B}_{k+1}^{n+1}$.

The solution of the magnetic field using (26) is a simple process. However, it should be noted that the ODE dealt here is different from a normal ODE where the derivatives of variables are usually taken with respect to time. In that case, the numerical solution of an ODE is to find the values of the unknown variables for a given time sequence, which is usually a known quantity and can be specified by the ODE solver. In choosing the time-step size, a large time step is desired to reduce the computational cost, but in the meantime, it must also be small enough to ensure both stability and accuracy. In (2), however, the derivative of $\mathbf{H}$ is taken with respect to $\mathbf{B}$, which is given by the estimated solution $\mathbf{A}$ from the TDFEM solver. Since the magnetic flux $\mathbf{B}$ is the unknown quantity, and its value at a specific point $\mathbf{r}$ is determined from the impressed current $\mathbf{J}_{\text{imp}}$ and the mutual coupling from all other points, there is no way that the step size $d\mathbf{B}$ can be controlled. As a result, given a $\mathbf{B}_k^{n+1}$ and the resulting $\Delta\mathbf{B}$, in order to achieve a prescribed accuracy, it is necessary to subdivide the step $\Delta\mathbf{B}$ into several smaller steps, and advance the solution step by step until the solution at $\mathbf{B}_k^{n+1}$ is obtained. Euler's method with subdivision is shown in Algorithm 1.

A simple example is given here to demonstrate the necessity of doing subdivision when using Euler's method to solve (2). Fig. 5 shows the hysteresis loops obtained from the inverse J-A model with $M_s = 1.168 \times 10^6\,\text{A/m}$, $a = 60\,\text{A/m}$, $k_p = 130\,\text{A/m}$, $\alpha = 10^{-4}$, and $c = 0.2$. Shown as the vertical axis in these two figures, the input magnetic flux is assumed to be a sinusoidal function in time, and

Input: The solutions from the previous time step: $\mathbf{B}^n$ and $\mathbf{H}^n$, the estimated solution of the current time step: $\mathbf{B}_k^{n+1}$, and the convergence criterion ϵ
Output: The magnetic field $\mathbf{H}_k^{n+1}$
Calculate the step $\Delta\mathbf{B} = \mathbf{B}_k^{n+1} - \mathbf{B}^n$;
Estimate the magnetic field using the original step $\mathbf{H} = \nu_0 \bar{\boldsymbol{\nu}}_r^d(\mathbf{B}^n,\mathbf{H}^n) \cdot \Delta\mathbf{B} + \mathbf{H}^n$;
for *Refinement* $i = 1, 2, 3, \ldots$ **do**
    Define number of subdivisions $L = 2^i$;
    Subdivide the step $\Delta\mathbf{B}_i = \Delta\mathbf{B}/L$;
    $\mathbf{B}_1 = \mathbf{B}^n$, $\mathbf{H}_1 = \mathbf{H}^n$;
    for *Subdivision* $j = 1, 2, \ldots, L$ **do**
        Advance the magnetic field with the subdivided step $\mathbf{H}_{j+1} = \nu_0 \bar{\boldsymbol{\nu}}_r^d(\mathbf{B}_j,\mathbf{H}_j) \cdot \Delta\mathbf{B}_i + \mathbf{H}_j$;
        Calculate $\mathbf{B}_{j+1} = \mathbf{B}_j + \Delta\mathbf{B}_i$;
    end
    if *The estimated field is converged* $\|\mathbf{H}_L - \mathbf{H}\|/\|\mathbf{H}\| < \epsilon$ **then**
        The magnetic field is obtained as $\mathbf{H}_k^{n+1} = \mathbf{H}_L$;
        Return $\mathbf{H}_k^{n+1}$;
    end
    Update the estimation $\mathbf{H} = \mathbf{H}_L$;
end

Algorithm 1: Euler's Method with Subdivision

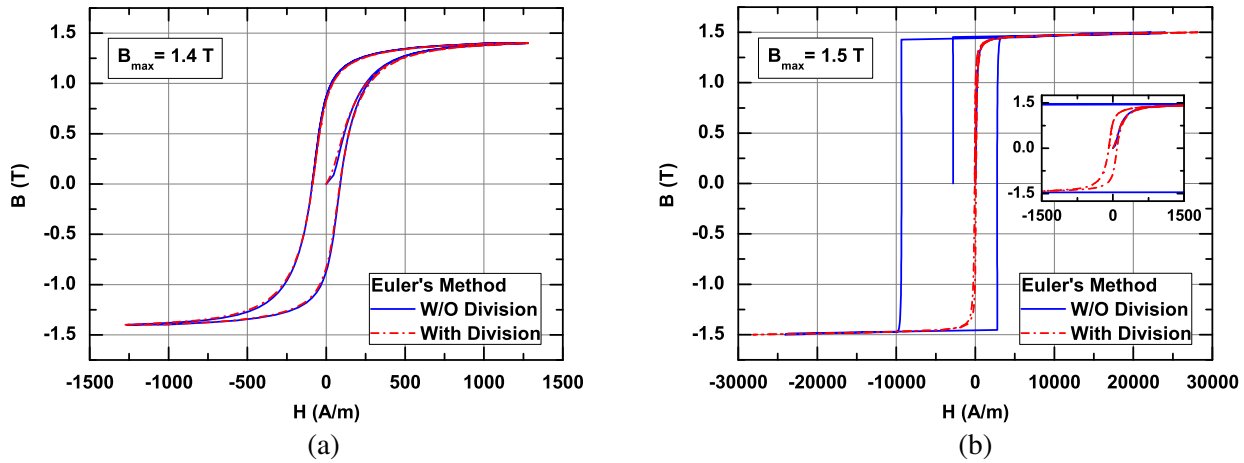

Figure 5. Hysteresis loops obtained by solving the ODE using Euler's method with and without subdivision when the magnitude of the magnetic flux is (a) 1.4 T and (b) 1.5 T.

its magnitude is $B_{\max} = 1.4\,\mathrm{T}$ in Fig. 5(a) and $B_{\max} = 1.5\,\mathrm{T}$ in Fig. 5(b). In order to solve the ODE using Euler's method, the time is divided uniformly into 150 time steps at which the magnetic flux is sampled and used as an input parameter of the ODE solver. From the figures, it is clear that when the magnitude of the magnetic flux is not very large, the numerical solutions obtained from Euler's method with and without subdivision almost overlap with each other. However, when the magnitude increases a little bit from 1.4 T to 1.5 T, Euler's method without subdivision would produce a numerical solution with an obvious error, while that with subdivision still reproduces the hysteresis loop well, as can be seen from the insert of Fig. 5(b).

3.2. Runge-Kutta Method

Euler's method discussed above is known as the single-step method since it only requires information at one point in time to advance the solution to the next time step. Because of this, the single-step method is also known as the "self-starting" method and is preferred in the solution of initial value problems (IVPs). However, since it comes from the first-order of the Taylor series expansion, Euler's method is only first-order accurate. As a result, it usually requires many loops of subdivisions to achieve a desired accuracy. If the true solution is varying rapidly, Euler's method becomes very inefficient. Considering the fact that the ODE has to be solved in every mesh element (tetrahedron, for example) of a geometry, or even at every Gaussian quadrature point of every element, the low-order accuracy of Euler's method will eventually become a bottleneck of the entire algorithm.

To achieve a higher-order accuracy and hence a better solution efficiency, the well-known Runge-Kutta method is adopted in this work. The Runge-Kutta method, which is another type of single-step method, uses the information from several intermediate auxiliary steps to form the solution with a higher-order accuracy. By expressing the higher-order Taylor series expansion in terms of the linear combination of the first-order derivatives at several intermediate steps, the Runge-Kutta method is able to achieve a higher-order accuracy without the need of evaluating higher-order derivatives. Since it requires information at several intermediate steps, the Runge-Kutta method is known as a multi-stage method.

There are many different variations of the Runge-Kutta method available in the literature. Here, only the most commonly used fourth-order Runge-Kutta method is considered. The fourth-order Runge-Kutta method, also known as the classical Runge-Kutta method, requires four evaluations of the first-order derivative $\bar{\boldsymbol{\nu}}_r^d$ to construct the fourth-order Taylor series expansion, as described in Algorithm 2. The classical Runge-Kutta method is proven to have a local truncation error of $\mathcal{O}(\Delta\mathbf{B}^5)$ and a global accumulated error of $\mathcal{O}(\Delta\mathbf{B}^4)$. As stated before, since the step size $\Delta\mathbf{B}$ is not directly controllable, it is necessary to subdivide $\Delta\mathbf{B}$ into several small steps, and advance the solution step by step to reduce the accumulated error and achieve a desired accuracy. The Runge-Kutta method with subdivision can

Input: The solutions from the previous time step: $\boldsymbol{B}^n$ and $\boldsymbol{H}^n$, the estimated solution of the current time step: $\boldsymbol{B}_k^{n+1}$, and the convergence criterion ϵ

Output: The magnetic field $\boldsymbol{H}_k^{n+1}$

1 Calculate the step $\Delta\boldsymbol{B} = \boldsymbol{B}_k^{n+1} - \boldsymbol{B}^n$;
2 Define the midpoint of the step as $\boldsymbol{B}_{\text{mid}} = \boldsymbol{B}^n + \Delta\boldsymbol{B}/2$;
3 Calculate the differential susceptibility using the fields at the previous time step $\bar{\boldsymbol{\nu}}_{r,1}^d = \bar{\boldsymbol{\nu}}_r^d\left(\boldsymbol{B}^n, \boldsymbol{H}^n\right)$;
4 Advance the magnetic field by half step using Euler's method with the differential susceptibility $\bar{\boldsymbol{\nu}}_{r,1}^d$ as $\boldsymbol{H}_1 = \nu_0 \bar{\boldsymbol{\nu}}_{r,1}^d \cdot \Delta\boldsymbol{B}/2 + \boldsymbol{H}^n$;
5 Calculate the differential susceptibility using $\boldsymbol{B}_{\text{mid}}$ and $\boldsymbol{H}_1$ as $\bar{\boldsymbol{\nu}}_{r,2}^d = \bar{\boldsymbol{\nu}}_r^d\left(\boldsymbol{B}_{\text{mid}}, \boldsymbol{H}_1\right)$;
6 Advance the magnetic field by half step using Euler's method with the differential susceptibility $\bar{\boldsymbol{\nu}}_{r,2}^d$ as $\boldsymbol{H}_2 = \nu_0 \bar{\boldsymbol{\nu}}_{r,2}^d \cdot \Delta\boldsymbol{B}/2 + \boldsymbol{H}^n$;
7 Calculate the differential susceptibility using $\boldsymbol{B}_{\text{mid}}$ and $\boldsymbol{H}_2$ as $\bar{\boldsymbol{\nu}}_{r,3}^d = \bar{\boldsymbol{\nu}}_r^d\left(\boldsymbol{B}_{\text{mid}}, \boldsymbol{H}_2\right)$;
8 Advance the magnetic field by full step using Euler's method with the differential susceptibility $\bar{\boldsymbol{\nu}}_{r,3}^d$ as $\boldsymbol{H}_3 = \nu_0 \bar{\boldsymbol{\nu}}_{r,3}^d \cdot \Delta\boldsymbol{B} + \boldsymbol{H}^n$;
9 Calculate the differential susceptibility using $\boldsymbol{B}_k^{n+1}$ and $\boldsymbol{H}_3$ as $\bar{\boldsymbol{\nu}}_{r,4}^d = \bar{\boldsymbol{\nu}}_r^d\left(\boldsymbol{B}_k^{n+1}, \boldsymbol{H}_3\right)$;
10 Define the effective differential susceptibility as $\bar{\boldsymbol{\nu}}_r^d = \left(\bar{\boldsymbol{\nu}}_{r,1}^d + 2\,\bar{\boldsymbol{\nu}}_{r,2}^d + 2\,\bar{\boldsymbol{\nu}}_{r,3}^d + \bar{\boldsymbol{\nu}}_{r,4}^d\right)/6$;
11 Calculate the magnetic field at the estimated flux $\boldsymbol{B}_k^{n+1}$ using Euler's method with the effective differential susceptibility as $\boldsymbol{H}_k^{n+1} = \nu_0 \bar{\boldsymbol{\nu}}_{\text{r}}^{\text{d}} \cdot \Delta\boldsymbol{B} + \boldsymbol{H}^n$;
12 Return $\boldsymbol{H}_k^{n+1}$.

Algorithm 2: The Fourth-Order Runge-Kutta Method

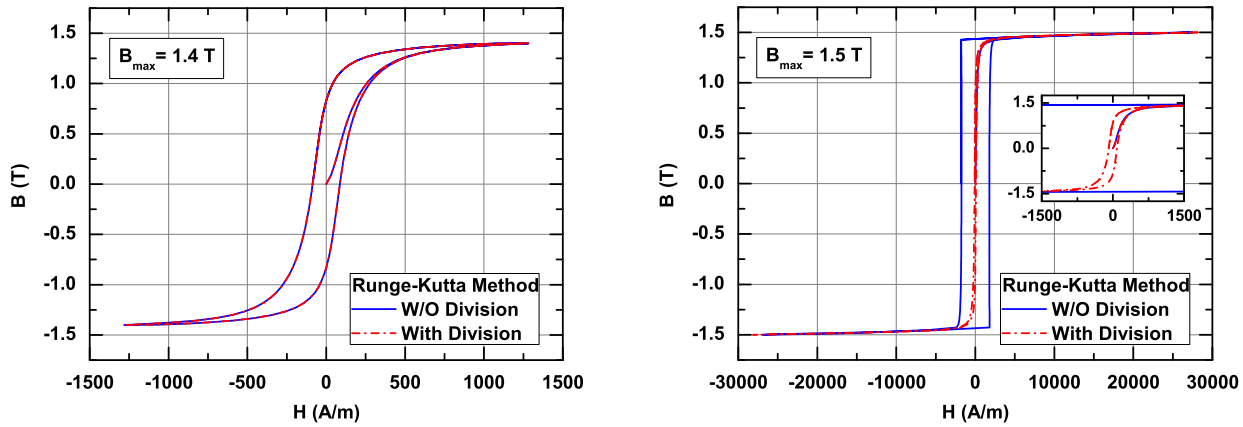

Figure 6. Hysteresis loops obtained by solving the ODE using the fourth-order Runge-Kutta method with and without subdivision when the magnitude of the magnetic flux is (a) 1.4 T and (b) 1.5 T.

be performed in a similar manner as shown in Algorithm 1, with a simple substitution of Lines 2 and 8 by the entire Algorithm 2.

To demonstrate its higher-order accuracy, the ODE with the same parameters shown in the preceding section is solved again in this section, using the fourth-order Runge-Kutta method with and without subdivision. The input magnetic flux is also assumed to be a sinusoidal function in time, which is divided uniformly into 150 time steps. The results using $B_{\max} = 1.4\,\text{T}$ and $B_{\max} = 1.5\,\text{T}$ are shown in Figs. 6(a) and 6(b), respectively. From the figures, it is clear that for the 1.4-T case, the numerical solutions obtained from the classical Runge-Kutta method with and without subdivision are identical to each other. However, when the magnitude increases from 1.4 T to 1.5 T, the Runge-Kutta

method without subdivision produces a numerical solution with an obvious error. Nevertheless, the error is smaller than that produced by the corresponding Euler's method, indicating a better numerical accuracy of the Runge-Kutta method. The Runge-Kutta method with subdivision still reproduces the hysteresis loop well, as can be seen from the insert of Fig. 6(b).

A further comparison made between Euler's and the Runge-Kutta methods with subdivision can be found in Figs. 7 and 8, and Tab. 3. From Fig. 7, it is clear that the results obtained from these two

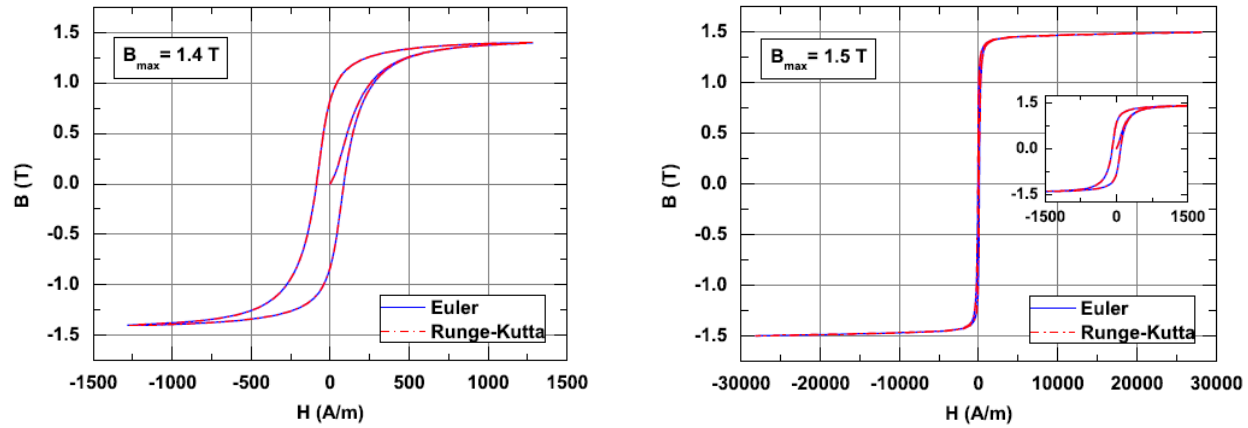

Figure 7. Comparison of the hysteresis loops obtained by solving the ODE using Euler's method and the fourth-order Runge-Kutta method with subdivision when the magnitude of the magnetic flux is (a) 1.4 T and (b) 1.5 T.

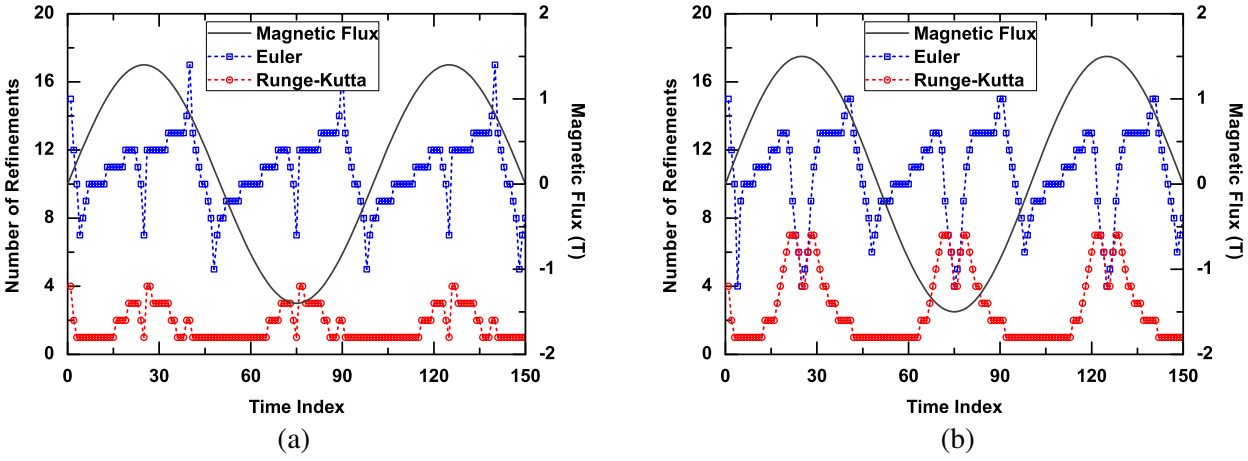

Figure 8. Number of step refinements required by solving the ODE using Euler's method and the fourth-order Runge-Kutta method with a desired accuracy set to be $\epsilon = 10^{-5}$ when the magnitude of the magnetic flux is (a) 1.4 T and (b) 1.5 T.

Table 3. Computational time of producing the hysteresis loop using different ode solvers with subdivision.

ODE Solver	$B_{\max} = 1.4\,\mathrm{T}$			$B_{\max} = 1.5\,\mathrm{T}$		
	$\epsilon = 10^{-4}$	$\epsilon = 10^{-5}$	$\epsilon = 10^{-6}$	$\epsilon = 10^{-4}$	$\epsilon = 10^{-5}$	$\epsilon = 10^{-6}$
Euler	11.86 s	105.34 s	984.03 s	9.13 s	86.23 s	989.44 s
Runge-Kutta	0.32 s	0.43 s	0.71 s	0.98 s	1.61 s	2.43 s

methods are identical, in both 1.4-T and 1.5-T cases. However, different computational efficiencies can be observed from Fig. 8, in which the numbers of step refinements R are shown at each step, with a desired accuracy set to be $\epsilon = 10^{-5}$. The total number of evaluations needed at each step is

$$N = \sum_{i=1}^{R} 2^i \tag{27}$$

which increases drastically when R increases. Tab. 3 shows the total computational time needed by these two methods in order to obtain the numerical solutions at all 150 field steps. From the table, it can be seen that the Runge-Kutta method has a much better computational efficiency. With the increased accuracy requirement, the computational time needed by Euler's method increases very rapidly, while that needed by the Runge-Kutta method increases only by a little.

4. BROYDEN'S METHODS FOR NONLINEAR PROBLEMS

The solution of a nonlinear equation with the Newton-Raphson method requires the repeated construction and solution of the Jacobian matrix, which can be very time-consuming for large problems. In this section, the multi-dimensional secant methods, Broyden's methods [7], are employed to accelerate the construction and solution of the Jacobian matrix equation.

4.1. Approximation of the Jacobian Matrix

In the original Newton-Raphson method, the Jacobian matrix needs to be updated at every Newton step using an appropriate formulation discussed in Section 2.2, and the Jacobian matrix (12) is then solved and the trial solution is updated using (13). In Broyden's methods, the Jacobian matrix is only calculated at the initial step. It is then approximated using a rank-one update at the successive steps, which are called Broyden steps in order to distinguish with the Newton steps where the Jacobian matrix is calculated explicitly.

At the kth Broyden step, the Jacobian matrix is approximated as the Broyden matrix

$$\mathbf{B}_k \approx \mathbf{J}_k. \tag{28}$$

To obtain the approximation at the $(k+1)$th Broyden step, the Broyden matrix can be updated with a rank-one matrix as

$$\mathbf{B}_{k+1} = \mathbf{B}_k + \mathbf{u}_k \mathbf{v}_k^t, \tag{29}$$

where the superscript t stands for transpose and $\mathbf{u}_k$ and $\mathbf{v}_k$ are column vectors defined as

$$\mathbf{u}_k = \frac{\mathbf{f}_{k+1}}{\|\mathbf{s}_k\|}; \quad \mathbf{v}_k = \frac{\mathbf{s}_k}{\|\mathbf{s}_k\|}. \tag{30}$$

In the above expression, $\mathbf{f}$ and $\mathbf{s}$ are the residual $\{r\}$ and the incremental solution $\{\delta a\}$ defined in (14) and (12), respectively. Equation (29) is the simplest approach of updating the Broyden matrix, and it satisfies the following conditions which justify its validation:

(i) The secant condition, which means the updated Broyden matrix satisfies

$$\mathbf{B}_{k+1}(\mathbf{x}_{k+1} - \mathbf{x}_k) = \mathbf{f}_{k+1} - \mathbf{f}_k. \tag{31}$$

(ii) The updated matrix $\mathbf{B}_{k+1}$ is the one closest to $\mathbf{B}_k$ in a sense of the Frobenius norm among all the matrices satisfying the secant condition.

Using (29), the approximated Jacobian matrix can be updated very efficiently. However, it still needs to be factorized and solved at every Broyden step, which is much more time consuming than the construction of the Jacobian matrix itself. As a result, the update of the inverse of the Jacobian matrix is preferred, which is discussed next.

4.2. Approximation of the Inverse Jacobian Matrix

As mentioned in the preceding section, the direct update of the inverse of the Jacobian matrix is more desired compared with the approximation of the Jacobian matrix itself. However, since the inversion of the Jacobian matrix would produce a fully populated matrix, it is more practical to update its product with a vector.

To construct such an inverse-matrix vector product, the well-known Sherman-Morrison formula can be used to express explicitly the inversion of a matrix with a rank-one update as

$$\left(\mathbf{B}+\mathbf{u}\mathbf{v}^t\right)^{-1}=\left(\mathbf{I}-\frac{\left(\mathbf{B}^{-1}\mathbf{u}\right)\mathbf{v}^t}{1+\mathbf{v}^t\mathbf{B}^{-1}\mathbf{u}}\right)\mathbf{B}^{-1}. \tag{32}$$

The Broyden matrix in (29) can therefore be inverted as

$$\mathbf{B}_{k+1}^{-1}=\left(\mathbf{B}_k+\mathbf{u}_k\mathbf{v}_k^t\right)^{-1}=\left(\mathbf{I}-\mathbf{w}_k\mathbf{v}_k^t\right)\mathbf{B}_k^{-1}, \tag{33}$$

where

$$\mathbf{w}_k=\frac{\mathbf{B}_k^{-1}\mathbf{u}_k}{1+\mathbf{v}_k^t\mathbf{B}_k^{-1}\mathbf{u}_k}. \tag{34}$$

At this moment, since there is no explicit form for $\mathbf{B}_k^{-1}$, it is still unclear how $\mathbf{B}_{k+1}^{-1}$ can be calculated. But it is clear that we can express $\mathbf{B}_k^{-1}$ by induction as

$$\mathbf{B}_k^{-1}=\prod_{j=0}^{k-1}\left(\mathbf{I}-\mathbf{w}_j\mathbf{v}_j^t\right)\mathbf{B}_0^{-1}. \tag{35}$$

The desired inverse-matrix vector product

$$\mathbf{s}_k=-\mathbf{B}_k^{-1}\mathbf{f}_k \tag{36}$$

can be obtained by applying the following steps:

(i) Solve for $\mathbf{z}_0$: $\mathbf{B}_0\mathbf{z}_0=-\mathbf{f}_k$;

(ii) Do: $\mathbf{z}_{j+1}=\mathbf{z}_j-\mathbf{w}_j\mathbf{v}_j^t\mathbf{z}_j$ for $j=0,1,\ldots,k-1$;

(iii) $\mathbf{s}_k=\mathbf{z}_k$.

Unfortunately, in the process described above, the vector $\mathbf{w}_j$ still involves the inverse of the Broyden matrix $\mathbf{B}_j^{-1}$, as indicated in (34). To compute $\mathbf{w}_j$, an auxiliary vector $\mathbf{p}$ is defined as

$$\mathbf{p}=\prod_{j=0}^{k-2}\left(\mathbf{I}-\mathbf{w}_j\mathbf{v}_j^t\right)\mathbf{B}_0^{-1}\mathbf{f}_k=\mathbf{B}_{k-1}^{-1}\mathbf{f}_k. \tag{37}$$

Then $\mathbf{s}_k$ can be rewritten as

$$\mathbf{s}_k=-\mathbf{B}_k^{-1}\mathbf{f}_k=-\left(\mathbf{I}-\mathbf{w}_{k-1}\mathbf{v}_{k-1}^t\right)\mathbf{p}=-\mathbf{p}+\mathbf{w}_{k-1}\mathbf{v}_{k-1}^t\mathbf{p}. \tag{38}$$

Invoking the definition of $\mathbf{u}_k$ in (30), we have

$$\mathbf{B}_{k-1}^{-1}\mathbf{u}_{k-1}=\mathbf{B}_{k-1}^{-1}\frac{\mathbf{f}_k}{\|\mathbf{s}_{k-1}\|}=\frac{\mathbf{p}}{\|\mathbf{s}_{k-1}\|}. \tag{39}$$

Therefore, by definition

$$\mathbf{w}_{k-1}=\frac{\mathbf{B}_{k-1}^{-1}\mathbf{u}_{k-1}}{1+\mathbf{v}_{k-1}^t\mathbf{B}_{k-1}^{-1}\mathbf{u}_{k-1}}=\frac{\mathbf{p}}{\|\mathbf{s}_{k-1}\|+\mathbf{v}_{k-1}^t\mathbf{p}}. \tag{40}$$

From (40) and (38), we have

$$\|\mathbf{s}_{k-1}\|\mathbf{w}_{k-1}=\mathbf{p}-\mathbf{w}_{k-1}\mathbf{v}_{k-1}^t\mathbf{p}=-\mathbf{s}_k, \tag{41}$$

which results in

$$\mathbf{w}_{k-1} = -\frac{\mathbf{s}_k}{\|\mathbf{s}_{k-1}\|}. \tag{42}$$

As a result, $\mathbf{B}_k^{-1}$ can eventually be expressed as

$$\mathbf{B}_k^{-1} = \prod_{j=0}^{k-1} \left(\mathbf{I} + \frac{\mathbf{s}_{j+1}\mathbf{s}_j^t}{\|\mathbf{s}_j\|^2} \right) \mathbf{B}_0^{-1} \tag{43}$$

after the application of (30). Since

$$\mathbf{s}_k = -\mathbf{B}_k^{-1}\mathbf{f}_k = -\left(\mathbf{I} + \frac{\mathbf{s}_k\mathbf{s}_{k-1}^t}{\|\mathbf{s}_{k-1}\|^2} \right) \mathbf{B}_{k-1}^{-1}\mathbf{f}_k, \tag{44}$$

it can be solved for $\mathbf{s}_k$ to obtain

$$\mathbf{s}_k = \mathbf{z}_{k-1} \left(1 - \frac{\mathbf{s}_{k-1}^t\mathbf{z}_{k-1}}{\|\mathbf{s}_{k-1}\|^2} \right)^{-1}, \tag{45}$$

where

$$\mathbf{z}_{j+1} = \mathbf{z}_j + \frac{\mathbf{s}_j^t\mathbf{z}_j}{\|\mathbf{s}_j\|^2}\mathbf{s}_{j+1} \quad (j = 0, 1, \ldots, k-2) \tag{46}$$

and

$$\mathbf{z}_0 = -\mathbf{B}_0^{-1}\mathbf{f}_k. \tag{47}$$

Obviously, in the solution of the nonlinear TDFEM using Broyden's method described above, the Broyden matrix only needs to be solved once, at the beginning of each time step. In order to achieve a better accuracy, the Jacobian matrix is usually constructed and solved explicitly at the first Broyden step of each time step. At the successive Broyden steps, the Jacobian matrix is approximated by the Broyden matrix and the inverse-matrix vector product is performed using (45)–(47). Since at each Broyden step, only the vectors $\mathbf{z}$ and $\mathbf{s}$ from the previous step are required, and the inversion term on the right-hand side of (45) is simply a scalar, the computation of the inverse-matrix vector product is very efficient.

4.3. Numerical Performance

To demonstrate the efficiency of Broyden's methods, we consider again TEAM problem 10 [22] used in Section 2.3.1. Since the first Broyden's method introduced in Section 4.1 only updates the Broyden matrix itself, the computational cost of solving the Broyden matrix equation is the same as that of solving the Jacobian matrix equation. Therefore, the second Broyden's method introduced in Section 4.2, where the inverse-matrix vector product is updated at each iteration, is applied to achieve a better efficiency. The results obtained from Broyden's method and that from the Newton-Raphson method are identical, and hence not shown here. Shown in Tab. 4 is the comparison of the computational costs by using the Newton-Raphson method versus Broyden's method. From the table, it is clear that by using Broyden's method, the total computational time has been reduced effectively to 45.8% of the total time required by the Newton-Raphson method. Nevertheless, it should also be noted that the average iteration count needed for the nonlinear solver to converge at each time step increases a little bit when Broyden's method

Table 4. Comparison of computational data for solving TEAM problem 10 using the Newton-Raphson (NR) and Broyden's (BD) methods.

$I_m = 5.64\,\mathrm{A}$	Δt (ms)	Total Time Steps	Ave. Iter. Per Time Step	Total CPU Time (s)
NR	3.0	50	3.04	425.77
BD	3.0	50	3.54	194.94

is employed. Such an increase in iteration count can be anticipated, because in theory Broyden's method only has a super-linear convergence, while the Newton-Raphson method has a quadratic convergence. This increase may become more serious when dealing with larger and more complicated problems. Therefore, Broyden's method needs to be applied with caution.

5. NONUNIFORM TIME-STEPPING SCHEME

The TDFEM solver discussed in the preceding sections is based on the application of the Newmark-β scheme, which is unconditionally stable and second-order accurate. However, the time-step size Δt is assumed to be a constant throughout the entire simulation process. To determine the time-step size in a nonlinear problem, several aspects need to be taken into consideration, including the operating frequency of the physical problem, the stability condition constrained by the temporal discretization scheme, and the convergence condition of the nonlinear solver. Under certain circumstances, nonuniform time-step sizes are more desirable in order to achieve a better accuracy and efficiency. In this section, the traditional Newmark-β scheme [8, 13, 14] with a uniform time-step size is generalized to a nonuniform scheme such that the total simulation steps can be significantly reduced.

Without the loss of generality, the nonuniform time-stepping scheme for the wave equation in the time domain can be obtained by deriving a recurrence formula for the ODE [8]

$$[M]\{\ddot{x}\} + [C]\{\dot{x}\} + [K]\{x\} + \{f\} = 0. \tag{48}$$

The unknown function $\{x\}$ is first expanded in terms of the temporal shape functions $N_i(t)$ in the time interval $[t_{n-1}, t_{n+1}]$

$$x(t) = \sum_{i=n-1}^{n+1} N_i(t) x_i, \tag{49}$$

which is then substituted into the ODE and tested with a weighting function $W(t)$ to yield

$$\int_{t_{n-1}}^{t_{n+1}} W \left[M \sum_i \ddot{N}_i x_i + C \sum_i \dot{N}_i x_i + K \sum_i N_i x_i + f \right] dt = 0. \tag{50}$$

By comparing the weak form (50) with the ODE (48), one can obtain that

$$\ddot{x}(t) = \sum_{i=n-1}^{n+1} \left(\int_{t_{n-1}}^{t_{n+1}} W \ddot{N}_i dt \right) x_i \tag{51}$$

$$\dot{x}(t) = \sum_{i=n-1}^{n+1} \left(\int_{t_{n-1}}^{t_{n+1}} W \dot{N}_i dt \right) x_i \tag{52}$$

$$x(t) = \sum_{i=n-1}^{n+1} \left(\int_{t_{n-1}}^{t_{n+1}} W N_i dt \right) x_i. \tag{53}$$

For a nonuniform time sequence $\{t_{n-1}, t_n, t_{n+1}\}$, define $\Delta t_1 = t_n - t_{n-1}$, $\Delta t_2 = t_{n+1} - t_n$, and $\Delta t_1 \neq \Delta t_2$. If the temporal shape functions are chosen as

$$N_{n-1} = \frac{(t - t_n)(t - t_{n+1})}{\Delta t_1 (\Delta t_1 + \Delta t_2)} \tag{54}$$

$$N_n = -\frac{(t - t_{n-1})(t - t_{n+1})}{\Delta t_1 \Delta t_2} \tag{55}$$

$$N_{n+1} = \frac{(t - t_{n-1})(t - t_n)}{(\Delta t_1 + \Delta t_2) \Delta t_2} \tag{56}$$

and the weighting function is chosen as

$$W(t) = \begin{cases} -\dfrac{t - t_n}{\Delta t_1}; & t \in [t_{n-1}, t_n] \\ \dfrac{t - t_n}{\Delta t_2}; & t \in [t_n, t_{n+1}], \end{cases} \tag{57}$$

the nonuniform time-stepping scheme is obtained as (after multiplied by $\Delta t_1 \Delta t_2$)

$$\ddot{x}(t) = \tilde{x}_{n+1} - 2\tilde{x}_n + \tilde{x}_{n-1} \tag{58}$$

$$\dot{x}(t) = \frac{1}{6}\{(-\Delta t_1 + 4\Delta t_2)\tilde{x}_{n+1} + 2(\Delta t_1 - \Delta t_2)\tilde{x}_n + (-4\Delta t_1 + \Delta t_2)\tilde{x}_{n-1}\} \tag{59}$$

$$x(t) = \frac{1}{12}\Big\{ [(\Delta t_1 + \Delta t_2)(-\Delta t_1 + 3\Delta t_2) - \Delta t_1 \Delta t_2]\, \tilde{x}_{n+1} + 2\left[(\Delta t_1 + \Delta t_2)^2 - \Delta t_1 \Delta t_2\right] \tilde{x}_n + [(\Delta t_1 + \Delta t_2)(3\Delta t_1 - \Delta t_2) - \Delta t_1 \Delta t_2]\, \tilde{x}_{n-1} \Big\}, \tag{60}$$

where

$$\tilde{x}_{n+1} = \Delta t_1 x_{n+1}; \quad \tilde{x}_n = \frac{\Delta t_1 + \Delta t_2}{2} x_n; \quad \tilde{x}_{n-1} = \Delta t_2 x_{n-1}. \tag{61}$$

Obviously, if $\Delta t_1 = \Delta t_2 = \Delta t$, the uniform Newmark-$\beta$ scheme with $\beta = 1/4$ is recovered.

To demonstrate the accuracy and efficiency of the proposed nonuniform time-stepping scheme, the same TEAM workshop problem 10 [22] is reconsidered. Since the excitation current is a dc current that is turned on from 0 A and gradually increased to I_m, the nonuniform time steps can be chosen such that the current increase between two consecutive time steps is constant. With this strategy, the nonuniform time steps are shown in Fig. 9(a). The average magnetic flux $\mathbf{B}$ in two different areas (S_1 and S_3) are recorded at these nonuniform time step points. The results from both the uniform (UT) and the nonuniform (NT) time-stepping schemes are shown and compared in Fig. 9(b). Both results agree very

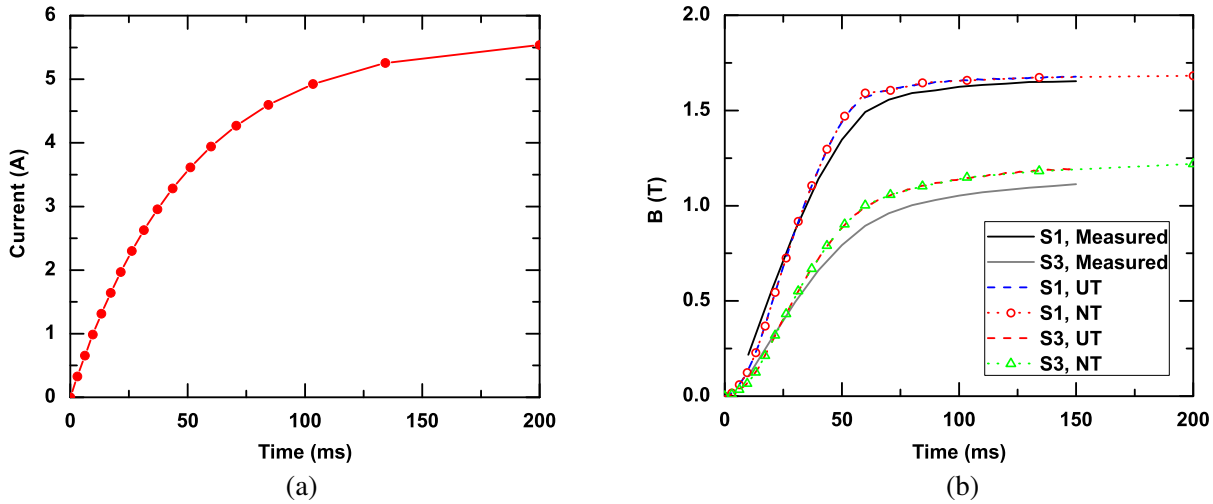

Figure 9. Numerical demonstration of the nonuniform time-stepping scheme through a benchmark problem, TEAM workshop problem 10. (a) Nonuniform time-step sizes. (b) Average magnetic flux density versus time in the observation areas S_1 and S_3. The observation areas are illustrated in Fig. 3(a) in [1]. Both numerical results obtained by the uniform (UT) and the nonuniform (NT) time-stepping schemes are shown.

Table 5. Comparison of computational data for solving TEAM problem 10 using the Newton-Raphson method with uniform time-stepping (UT) versus nonuniform time-stepping (NT).

$I_m = 5.64$ A	Δt (ms)	Total Time Steps	Total Physical Time (ms)	Total CPU Time (s)
UT	3.0	50	150	425.77
NT	N/A	17	200	166.08
BD + NT	N/A	17	200	86.97

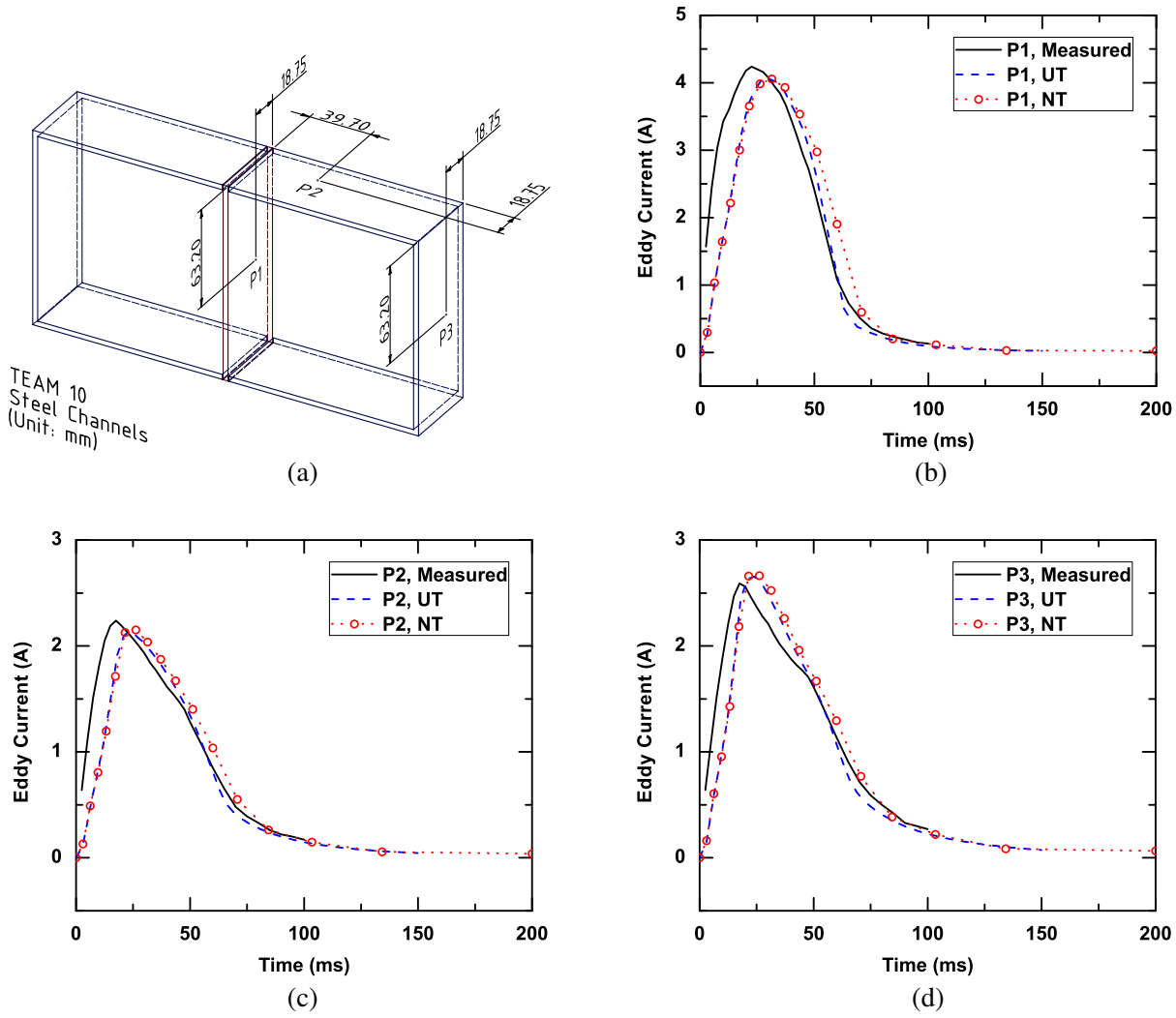

Figure 10. Numerical demonstration of the nonuniform time-stepping scheme through a benchmark problem, TEAM workshop problem 10. (a) Observation points on the steel channels. Eddy current versus time at the observation points (b) P_1, (c) P_2 and (d) P_3 are recorded and compared with the measurement data. Both numerical results obtained by the uniform (UT) and the nonuniform (NT) time-stepping schemes are shown.

well with the measurement. The eddy current $\mathbf{J}_e = \sigma\mathbf{E}$ induced in the steel structure is also recorded at three observation points shown in Fig. 10(a). From Figs. 10(b)–10(d), it is clear that both results obtained from the uniform and the nonuniform time-stepping schemes agree well with the measurement. Their computational data are presented in Tab. 5, from which it can be seen that the computational time needed by the nonuniform time-stepping scheme for the simulation of a 200-ms physical process is only 39% of that by the uniform time-stepping scheme for the simulation of a 150-ms physical process. Clearly, using the proposed nonuniform time-stepping method, nonlinear magnetic problems can be solved with a good accuracy and a better efficiency. What is more interesting is that the nonuniform time-stepping scheme can be used in combination with Broyden's methods to further accelerate the computation. Also presented in Tab. 5 is the computational time needed by the hybridization of Broyden's methods and the nonuniform time-stepping scheme. The total computational time is further reduced to 20% of the that needed by the original Newton-Raphson method with a uniform time-stepping scheme.

6. NUMERICAL EXAMPLES

In this section, numerical examples are given to demonstrate the capability of the proposed methods in the simulation of magnetic hysteresis problems. The nonlinear magnetic constitutive relation is represented by the inverse J-A vector model introduced in Section 2.1, and the resulting ODE is solved using the fourth-order Runge-Kutta method with subdivision presented in Section 3.2. The nonlinear magnetic problem is solved with the Newton-Raphson scheme described in Section 2.2.

6.1. Generation of Higher-order Harmonics

The phenomenon of magnetic hysteresis and the generation of higher-order harmonics are investigated using a three-limbed ferromagnetic plate adopted from TEAM workshop problem 32 [23]. As shown in Fig. 11, the plate is made of five layers of 0.48-mm-thick Fe-Si 3.2% wt laminations which has a conductivity of $\sigma = 1.78 \times 10^6$ S/m. The magnetic property is modeled by the inverse J-A model with

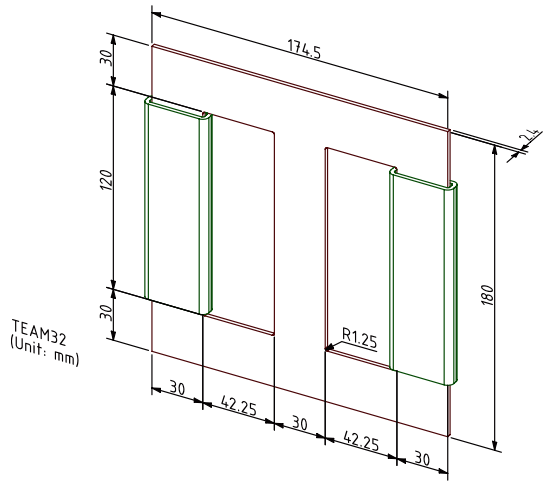

Figure 11. Problem setting and dimensions of the ferromagnetic core in TEAM problem 32.

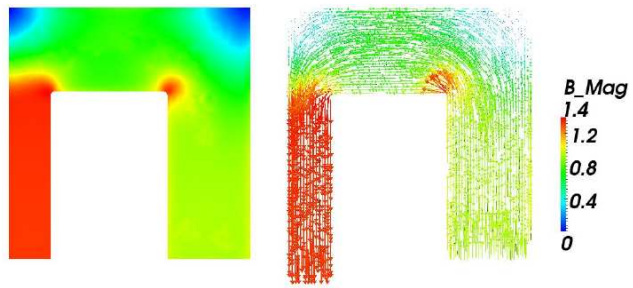

Figure 12. Magnetic flux density distribution on the ferromagnetic core (only one fourth is shown due to symmetry).

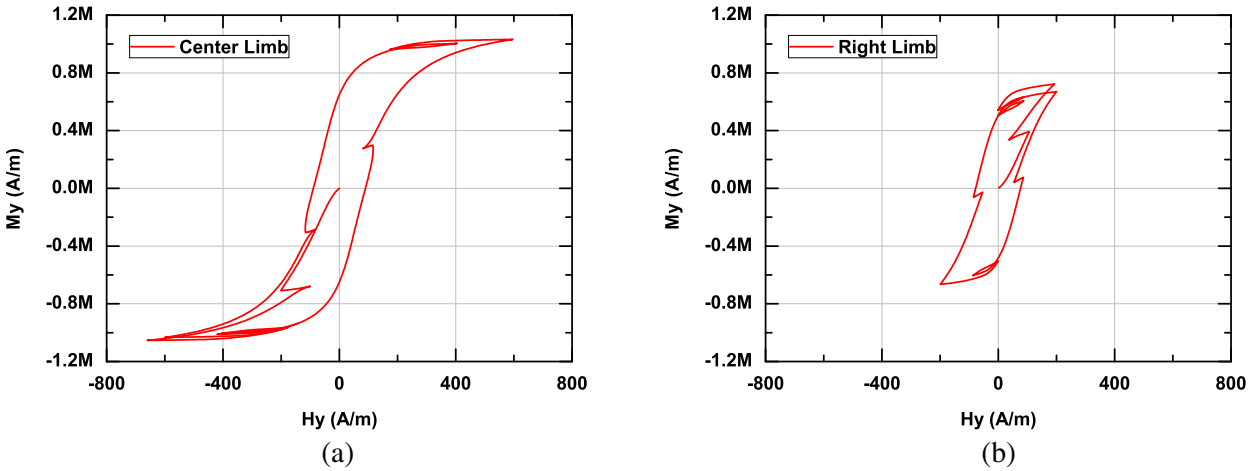

Figure 13. Numerical results of TEAM problem 32 solved by the nonlinear TDFEM formulation with a Newton-Raphson scheme and inverse J-A hysteresis model. (a) Hysteresis loop observed at the center of the center limb. (b) Hysteresis loop observed at the center of the right limb.

the model parameters chosen as $M_s = 1.168 \times 10^6$ A/m, $a = 60$ A/m, $k_p = 130$ A/m, $\alpha = 10^{-4}$, and $c = 0.2$. The excitation of this structure is supplied by two 90-turn windings placed on the external limbs. In this example, the winding current composes of a fundamental and a fifth harmonic with a maximum magnitude of 1.5 A, which can be expressed as

$$I = \sin(2\pi f_1 t) + 0.5\sin(2\pi f_5 t), \tag{62}$$

where $f_1 = 10$ Hz and $f_5 = 50$ Hz. Under such an excitation, the magnetic flux density is solved and a snapshot of the flux distribution is shown in Fig. 12. From the vector plot of this figure, it can be seen that the magnetic flux follows the right-hand rule, and the field singularities can be observed at the corners of the structure. The time-domain results of the magnetization **M** and the magnetic field **H** are recorded at the center of the center and the right limbs. The hysteresis loops at these two locations are shown in Fig. 13. From these two figures, both major and minor loops can be observed clearly. This problem is solved using both the Newton-Raphson and Broyden's methods. Both methods produce the same results, but Broyden's method only consumes 33.9% of the computational time needed by the Newton-Raphson method.

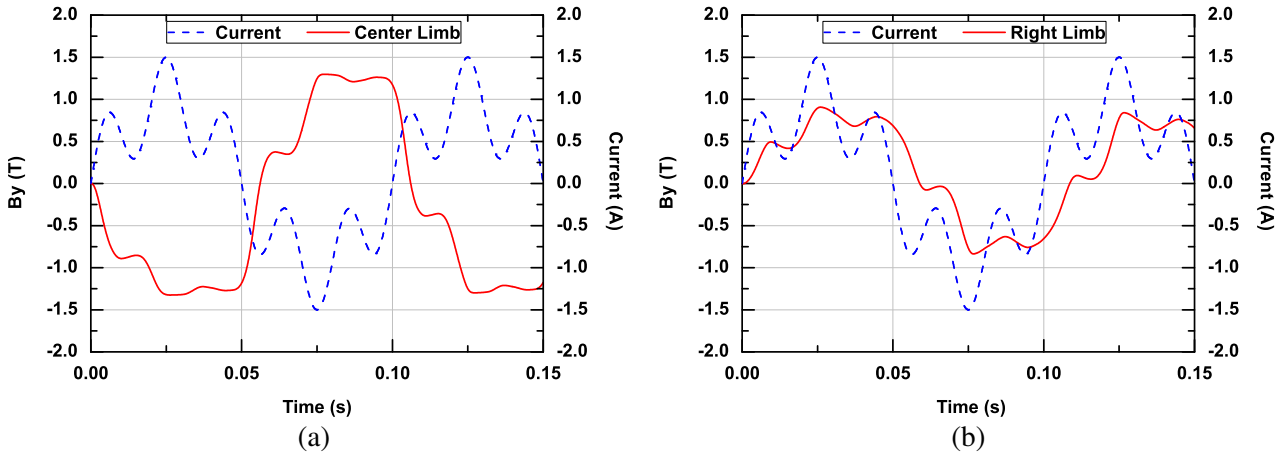

Figure 14. Numerical results of TEAM problem 32 solved by the nonlinear TDFEM formulation with a Newton-Raphson scheme and inverse J-A hysteresis model. (a) Magnetic flux density versus time at the center of the center limb. (b) Magnetic flux density versus time at the center of the right limb.

Shown in Fig. 14 is the winding current and the magnetic flux at the two observation points versus time. The time-domain results are then converted using the Fourier transform into the frequency domain to demonstrate the generation of higher-order harmonics. As can be seen in Fig. 15, the winding current only has a power spectrum at 10 Hz and 50 Hz, as specified in (62). Due to the nonlinearity, the corresponding magnetic flux has a more complicated power spectrum, which contains not only that of the winding current, but also the integer multiple and combinations of the input spectrum. Because of the constructive and destructive effect of the two input frequencies, the magnitudes of the newly generated higher-order harmonics are not decreasing monotonically, but exhibit complicated relations. From this example, it is clear that the higher-order harmonics can be accurately captured by using the proposed nonlinear solver.

6.2. Demagnetization Process and Magnetic Remanence

For time-harmonic nonlinear problems, the higher-order harmonics can also be calculated with a frequency-domain solver using the harmonic balance method [24]. However, for a transient problem, the harmonic balance method cannot be applied easily, because the response will have a continuous spectrum. One example of such a problem is the demagnetization problem discussed in this section. In the demagnetization process, an oscillating field with a center frequency of 10 Hz and a reducing amplitude is applied to remove the magnetization from the structure, causing the magnetic dipoles in

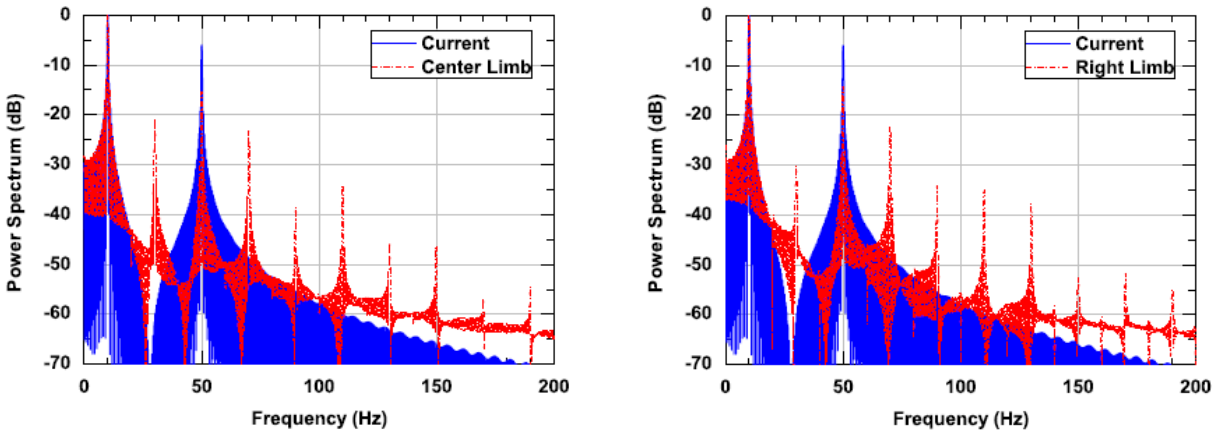

Figure 15. Power spectrum distribution of the excitation current and the responding magnetic flux at (a) the center limb and (b) the right limb.

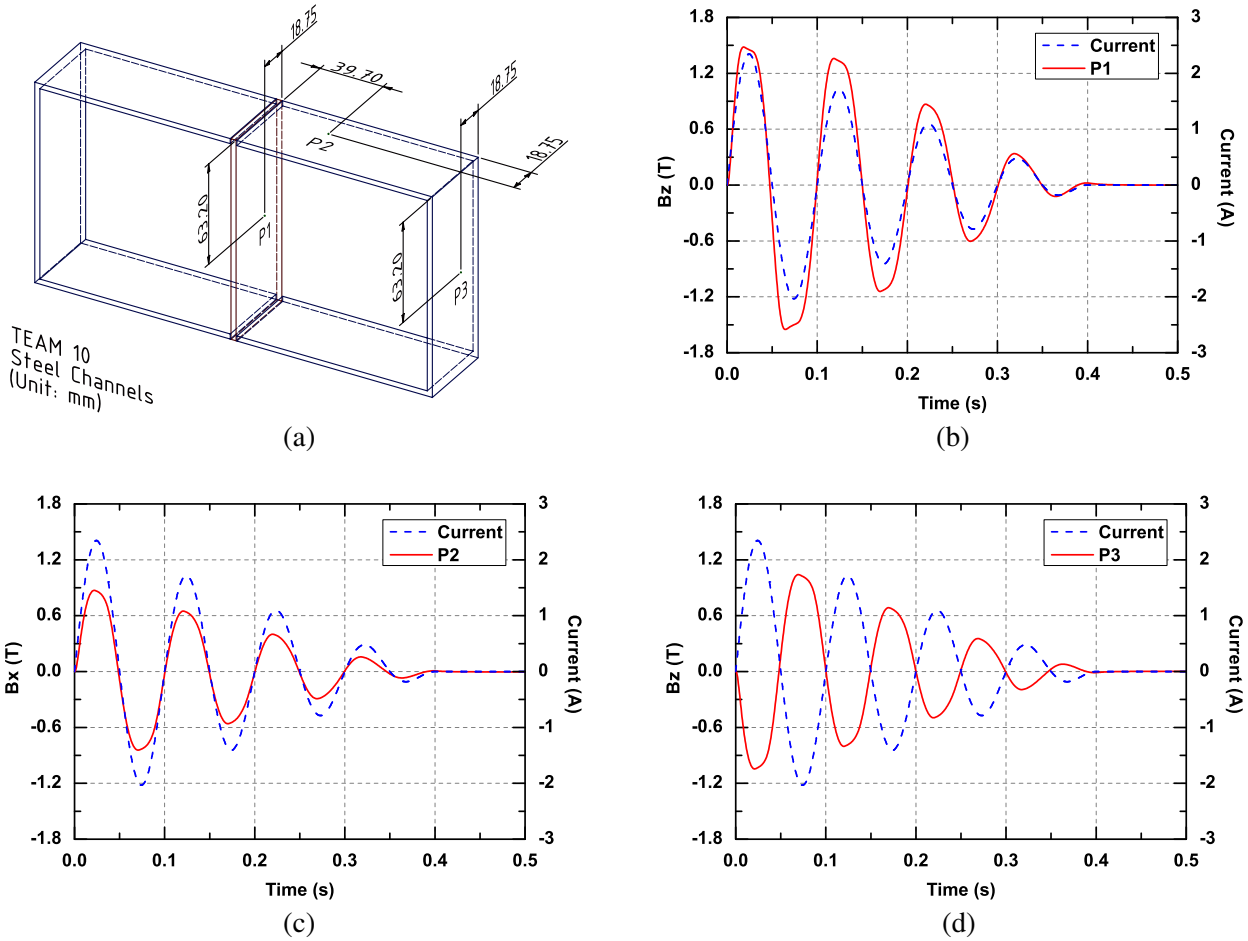

Figure 16. Numerical results of the nonlinear demagnetization problem solved by the nonlinear TDFEM formulation with a Newton-Raphson scheme. (a) Observation points on the steel channels. (b)–(d) Magnetic flux density versus time at the three observation points P_1–P_3.

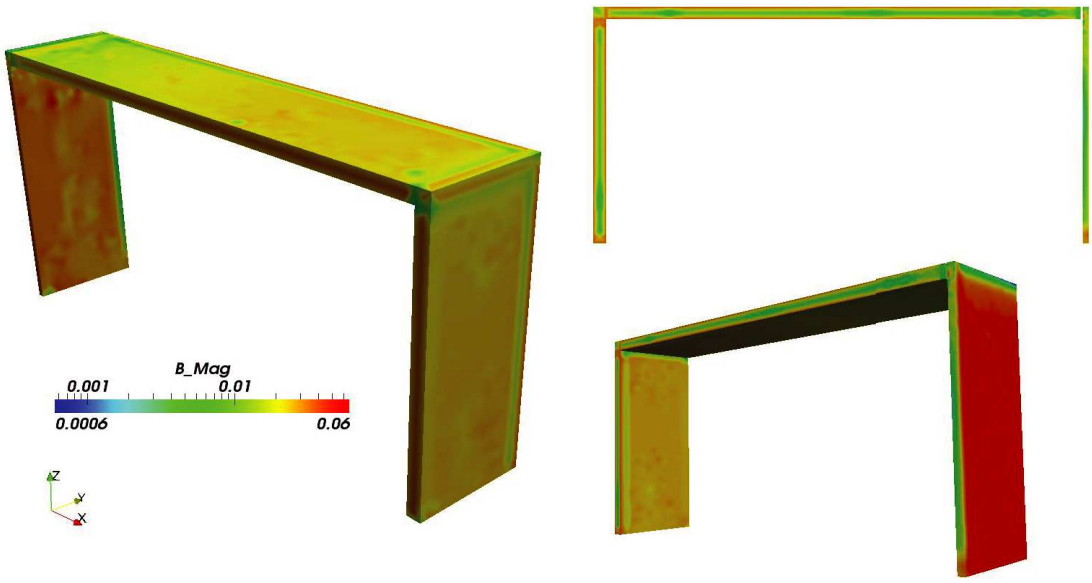

Figure 17. Magnetic remanence distribution at the end of the demagnetization process.

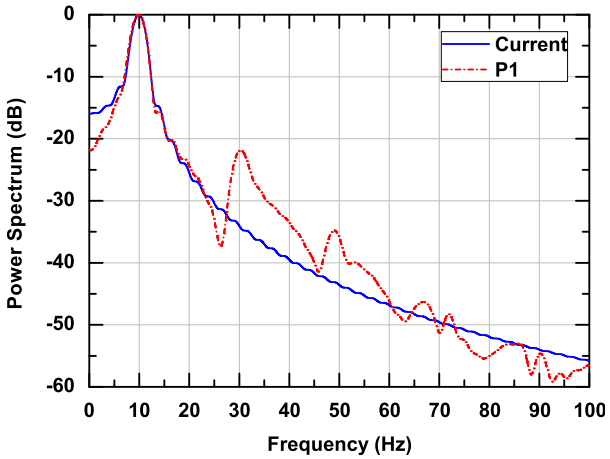

Figure 18. Power spectrum distribution of the excitation current and the responding magnetic flux at P_1.

the ferromagnetic material to flip back and forth and get neutralized. The model from TEAM workshop problem 10 [22] is used to demonstrate this process. To model the ferromagnetic material, the inverse J-A model is used, where the model parameters are chosen as $M_s = 1.3 \times 10^6$ A/m, $a = 25.3$ A/m, $k_p = 66.6$ A/m, $\alpha = 0$, and $c = 0.2$. The magnetic flux $\mathbf{B}$ at three different observation points (P_1, P_2, and P_3) in Fig. 16(a) are recorded and shown in Figs. 16(b)–16(d), as a function of time. Because of the location difference, among the three observation points, only the steel at point P_1 has been fully saturated by the externally applied current. The magnetic remanence at the end of the demagnetization process is shown in Fig. 17 from three different view angles. Also, from the power spectrum distribution of the coil current and the corresponding magnetic flux at the observation point P_1 shown in Fig. 18, it is clear that when the input current has a continuous spectrum, the response also has a continuous spectrum, which is difficult to simulate with the harmonic balance method in frequency domain. This demonstrates the significance of the time-domain method in the simulation of a real physical problem.

7. CONCLUSION

In this work, numerical solution of nonlinear magnetic problems was presented using a time-domain finite element method with an advanced magnetic hysteresis model in three dimensions. Accurate numerical solutions were obtained very efficiently using the proposed solver for ordinary differential equations representing the nonlinear constitutive relation. The vector curl-curl equation was formulated in the time domain with the magnetic vector potential employed as the unknown function, and the resulting nonlinear system was solved using both the Newton-Raphson and the fixed-point methods. In order to improve the computational efficiency, Broyden's methods and the nonuniform time-stepping technique were developed and implemented. The performances of these methods and techniques were demonstrated and compared through several well-acknowledged numerical examples. It was found out that with Broyden's methods, the computation can be accelerated by 2 to 3 times compared with the Newton-Raphson method. The restriction of the time-step sizes was successfully removed by the nonuniform time-stepping scheme, which resulted in a 2.5 times speed-up on the Newton-Raphson method. When Broyden's method and the nonuniform time-stepping scheme were used together, the total computational time was further reduced. The applications in the simulation of magnetic hysteresis and demagnetization process were shown, and the prediction of the harmonic generation was also presented. With all these techniques equipped, the proposed nonlinear time-domain finite element solver is able to solve nonlinear magnetic problems with a high efficiency and a good accuracy.

ACKNOWLEDGMENT

This work was supported in part by a grant from Sandia National Laboratories, a grant from National University of Singapore, and in part by the National Science Foundation of China (NSFC) under Contract No. 61201012, and the Fundamental Research Funds for the Central Universities under Contract No. ZYGX2012J016.

REFERENCES

1. Yan, S. and J.-M. Jin, "Theoretical formulation of a time-domain finite element method for nonlinear magnetic problems in three dimensions (Invited Paper)," in *the Commemorative Collection on the 150-Year Anniversary of Maxwell's Equations*, *Progress In Electromagnetics Research*, Vol. 153, 33–55, 2015.
2. Jin, J.-M., *The Finite Element Method in Electromagnetics*, 3rd edition, Wiley, Hoboken, NJ, 2014.
3. Jiles, D. C. and D. L. Atherton, "Theory of the magnetisation process in ferromagnetics and its application to the magnetomechanical effect," *J. Phys. D: Appl. Phys.*, Vol. 17, No. 6, 1265–1281, Jun. 1984.
4. Jiles, D. C. and D. L. Atherton, "Theory of ferromagnetic hysteresis," *Journal of Magnetism and Magnetic Materials*, Vol. 61, 48–60, Sep. 1986.
5. Bergqvist, A. J., "A simple vector generalization of the Jiles-Atherton model of hysteresis," *IEEE Trans. Magn.*, Vol. 32, No. 5, 4213–4215, Sep. 1996.
6. Leite, J. V., N. Sadowski, P. Kuo-Peng, N. J. Batistela, J. P. A. Bastos, and A. A. de Espindola, "Inverse Jiles-Atherton vector hysteresis model," *IEEE Trans. Magn.*, Vol. 40, No. 4, 1769–1775, Jul. 2004.
7. Broyden, C. G., "A class of methods for solving nonlinear simultaneous equations," *Math. Comp.*, Vol. 19, 577–593, 1965.
8. Zienkiewicz, O. C., "A new look at the Newmark, Houboult and other time stepping formulas: A weighted residual approach," *Earthquake Engineering and Structural Dynamics*, Vol. 5, 413–418, 1977.
9. Ren, Z., "Influence of the R.H.S. on the convergence behaviour of the curl-curl equation," *IEEE Trans. Magn.*, Vol. 32, No. 3, 655–658, May 1996.

10. Whitney, H., *Geometric Integration Theory*, Princeton University Press, Princeton, NJ, 1957.
11. Nédélec, J. C., "Mixed finite elements in R3," *Numer. Meth.*, Vol. 35, 315–341, 1980.
12. Webb, J. P., "Hierarchal vector basis functions of arbitrary order for triangular and tetrahedral finite elements," *IEEE Trans. Antennas Propag.*, Vol. 47, No. 8, 1244–1253, Aug. 1999.
13. Newmark, N. M., "A method of computation for structural dynamics," *J. Engineering Mechanics Division. ASCE*, Vol. 85, 67–94, Jul. 1959.
14. Gedney, S. D. and U. Navsariwala, "An unconditionally stable finite element time-domain solution of the vector wave equation," *IEEE Microw. Guided Wave Lett.*, Vol. 5, No. 10, 332–334, Oct. 1995.
15. Peterson, A. F., "Absorbing boundary conditions for the vector wave equation," *Microw. Opt. Tech. Lett.*, Vol. 1, No. 2, 62–64, 1988.
16. Webb, J. P. and V. N. Kanellopoulos, "Absorbing boundary conditions for the finite element solution of the vector wave equation," *Microw. Opt. Tech. Lett.*, Vol. 2, No. 10, 370–372, 1989.
17. "Testing electromagnetic analysis methods (T.E.A.M.)," http://www.compumag.org/jsite/team.html, International Compumag Society.
18. Albanese, R. and G. Rubinacci, "Solution of three dimensional eddy current problems by integral and differential methods," *IEEE Trans. Magn.*, Vol. 24, 98–101, Jan. 1998.
19. Lee, S. H., "Efficient finite element electromagnetic analysis for high-frequency/high-speed circuits and multiconductor transmission line," Ph.D. dissertation, University of Illinois at Urbana-Champaign, Urbana, IL, USA, 2009.
20. Jorgensen, E., J. L. Volakis, P. Meincke, and O. Breinbjerg, "Higher order hierarchical Legendre basis functions for electromagnetic modeling," *IEEE Trans. Antennas Propag.*, Vol. 52, No. 11, 2985–2995, Nov. 2004.
21. Nakata, T., T. Takahashi, K. Fujiwara, and P. Olszewski, "Analysis of magnetic fields of 3-D nonlinear magnetostatic model (problem 13)," *Proc. of the European TEAM Workshop and Int. Sem. on Elecmagn. Field Anal.*, Oxford, England, Apr. 1990.
22. Nakata, T., N. Takahashi, and K. Fujiwara, "Summary of results for benchmark problem 10 (steel plates around a coil)," *Compel.*, Vol. 14, No. 2/3, 103–112, Sep. 1995.
23. Bottauscio, O., M. Chiampi, C. Ragusa, L. Rege, and M. Repetto, "A test-case for validation of magnetic field analysis with vector hysteresis," *IEEE Trans. Magn.*, Vol. 38, No. 2, 893–896, Mar. 2002.
24. Yamada, S., K. Bessho, and J. Lu, "Harmonic balance finite element method applied to nonlinear AC magnetic analysis," *IEEE Trans. Magn.*, Vol. 24, No. 4, 2971–2973, Jul. 1989.